



INVESTIGATION OF HEAT TRANSFER IMPROVEMENTS OF GRAPHENE OXIDE-WATER AND DIAMOND-WATER NANOFLUIDS IN CROSS-FLOW-IMPINGING JET FLOW CHANNELS HAVING FIN

Koray KARABULUT

Sivas Cumhuriyet University, Sivas Technical Sciences Vocational School, Department of Electric and Energy
Sivas, Turkey

kkarabulut@cumhuriyet.edu.tr, ORCID: 0000-0001-5680-0988

(Geliş Tarihi: 18.09.2022, Kabul Tarihi: 27.02.2023)

Abstract: In this study, the heat transfer from two different model surfaces (roof and crown) and flow structure in the channels with the cross flow-impinging jet flow were numerically analyzed by using water, 0.02% GO (Graphene Oxide)-Water and 2% Diamond-Water nanofluids. The numerical study was carried out steady and three dimensional using the Ansys-Fluent program with k-ε turbulence model. A fin with 90° angle was added on the upper channel surface from the impinging jet inlet at distinct distances. A constant heat flux of 1000 W/m² was applied to the model surfaces. The channel heights are fixed and the Re range of the fluids is 5000-15000. The numerical results obtained from the study were compared with the results of the experimental studies in the literature and it was seen that the results were compatible and acceptable. The results of the study were comparatively examined for water and nanofluids as the mean Nu and surface temperature variations for each model in the channels without fins and at different fin distances. Also, velocity and temperature contour distributions of the combined jet Diamond-Water nanofluid flow were visualized. However, performance coefficient (C) and mean Nu (Nu_m) and, surface temperature values (T_m) were evaluated for all three patterned surfaces in the channels. Nu_m increases for GO-Water nanofluid at Re=15000 and fin distance of 2D are 47.53% and 57.42% compared to the case of using finless and water fluid for the roof and crown model surfaces, respectively.

Keywords: Cross flow-impinging jet flow, Carbon-based nanofluid, Fin, Heat transfer.

KANATÇIKLI ÇAPRAZ-AKIŞ-ÇARPAN JET AKIŞLI KANALLARDA GRAFEN OKSİT-SU VE ELMAS-SU NANOAKIŞKANLARININ ISI TRANSFERİ İYİLEŞTİRMELERİNİN ARAŞTIRILMASI

Özet: Bu çalışmada, çapraz akış-çarpın jet akışlı kanallarda iki farklı model yüzeyinden (çatı ve taç) olan ısı transferi ve akış yapısı su, %0,02 GO (Grafen Oksit)-Su ve %2 Elmas-Su nanoakışkanları kullanılarak sayısal olarak analiz edilmiştir. Sayısal çalışma, k-ε türbülans modelli Ansys-Fluent programı kullanılarak sürekli ve üç boyutlu olarak gerçekleştirilmiştir. Kanal üst yüzeyine çarpın jet girişinden itibaren farklı mesafelerde 90° açılı bir kanatçık eklenmiştir. Model yüzeylerine 1000 W/m² lik bir sabit ısı akısı uygulanmıştır. Kanal yükseklikleri sabittir ve akışkanların Re sayısı aralığı 5000-15000' dir. Çalışmadan elde edilen sayısal sonuçlar, literatürdeki çalışmanın deneysel sonuçlarıyla karşılaştırılmış ve sonuçların makul ve kabul edilebilir olduğu görülmüştür. Sonuçlar, kanatçiksız ve farklı kanatçık uzaklıklarında kanallardaki her bir model için ortalama Nu sayısı ve yüzey sıcaklık değişimleri şeklinde su ve nanoakışkanlar için karşılaştırmalı olarak incelenmiştir. Ayrıca, birleşik jet Elmas-Su nanoakışkan akışının hız ve sıcaklık konturu dağılımları görselleştirilmiştir. Bununla birlikte, performans katsayısı (C) ve ortalama Nu (Nu_m) ve yüzey sıcaklık değerleri (T_m) kanallarda bulunan her üç desenli yüzey için değerlendirilmiştir. Re=15000 ve 2D kanatçık uzaklığında GO-Su nanoakışkan için Nu_m artışları, kanatçiksız ve su akışkanları kullanılan durumla kıyaslandığında çatı ve taç model yüzeyleri için sırasıyla %47,53 ve %57,42' dir.

Anahtar Kelimeler: Çapraz akış-çarpın jet akışı, Karbon tabanlı nanoakışkan, Kanatçık, Isı transferi.

NOMENCLATURE

A _c	Cross-sectional area of the channel [m ²]	W	Width of the channel [mm]
C	Performance Coefficient [=Nu/ΔP]	H	Height of the channel [mm]
D	Jet inlet diameter [mm]	m	One side length of the model [mm]
L	Length of the channel [mm]	P _c	Wet area of the channel [m ²]
		θ	Fin angle [°]
		f	Friction factor [=2ΔPD/ρLV ²]

h	Heat convection coefficient [$\text{W}/\text{m}^2\text{K}$]
k_f	Thermal conductivity of the fluid [W/mK]
V	The velocity of the fluid at the inlet of the channel [m/s]
c_p	Specific heat of the fluid [J/kgK]
p	Pressure [Pa]
q''	Heat flux on model surfaces [W/m^2]
N	Distance of fin from jet inlet [mm]
T	Temperature [K]
u_i	Velocity components in x , y and z coordinates [m/s]
Re	Reynolds number [$=\rho VD/\mu$]
Nu	Nusselt number [$=hL/k$]
μ	Dynamic viscosity [kg/sm]
μ_t	Turbulent viscosity [kg/sm]
ν	Kinematic viscosity [m^2/s]
ρ	Density of the fluid [kg/m^3]
k	Kinetic energy of turbulent flow [m^2/s^2]
ϵ	Turbulent dissipation rate [m^2/s^3]

Subscripts

atm	Atmosphere
bf	Base fluid (Water)
c	Channel
f	Fluid
h	Hydraulic
j	Jet
m	Mean
nf	Nanofluid
o	Outlet
p	Nanoparticle
s	Surface

INTRODUCTION

Conservation of energy and the development of alternative energy sources are the biggest problems nowadays. Although traditional energy resources are expected to be exhausted in the next twenty to thirty years, energy wars are also on the agenda of the world's countries. Therefore, energy should be used economically and efficiently in all areas.

With traditional and inefficient heat transfer methods, more energy is consumed and sufficient and desired heat transfer performance cannot be achieved (Naga Ramesh et al., 2021). The cross-flow cooling method, which is used to increase heat transfer from electronic elements, is one of the most widely used methods. This method is based on the principle of sending the cold fluid over all the components with a fan, thereby cooling the entire electronic components. However, since this method is based on cooling all circuit elements, it may fail to transfer heat from components at very high temperatures. Another method of heat transfer is impinging jet cooling. In this method, cold fluid is locally sprayed onto an element with a high temperature by a nozzle. While a high-temperature circuit

component can be cooled with the impinging jet, it may be insufficient in cooling the entire circuit. However, there are multiple elements in an electronic circuit whose temperatures are quite different from each other. For this reason, it is difficult to reach the conditions that can keep the whole circuit safely with a single type of cooling method. Implementing the impinging jet and cross-flow cooling method together and applying it as a combined jet flow (cross flow and impinging jet) can create a beneficial situation with high cooling capacity. While the circuit elements as a whole can be cooled to a certain temperature level with cross-flow, only the very high-temperature elements in the circuit can be cooled pointwise by the impinging jet flow (Kılıç, 2018; Teamah et al., 2015).

In the literature, there are many studies evaluating only cross flow or only jet flow. Since the model examined in this study is more like jet flow, the literature review focused more on jet flow. However, many numerical and experimental studies on impinging jets exist in the literature. In these studies, the effects of variables such as the type of fluid used for the impinging jets, the geometry of the flow area, the turbulence model, the Re value, the jet distance and the heat flux on the heat transfer from the circuit components were investigated. In addition, studies on cooling methods in which cross flow and impinging jet flow are used together are limited, regarding the directing of the fluid to the heated surfaces in the channel, as researched in this study, a study in which detailed channel and heated surface designs are used and carbon-based GO-Water and Diamond-Water nanofluids, the importance and use of which have been increasing in recent years, have not been found in the literature.

The flow and heat transfer properties of an impinging circular jet flow on a concave surface with constant heat flux were investigated numerically and experimentally by Hadipour and Zargarabadi (2018) at different jet-to-plate ratios. The effects of different H/D (channel height/jet inlet diameter) ratios, Re values and jet diameter values were investigated and it was seen that the heat transfer increased with the increase in jet diameter at a constant Re . Karabulut and Alnak (2021) numerically investigated the cooling of copper plate surfaces in rectangular ducts with two different patterns in the form of roof and trapezoidal with a single air jet flow at different jet inlet widths. While the jet inlet widths were $0.5 D_h$ and D_h , the distances between the jet and the plate (H/D_h) were 3 and 6. As a result, they determined that at $0.5 D_h$ jet width, $H/D_h=6$, and $Re=5000$, the mean Nu value was 25.92% higher on the roof patterned surface than on the trapezoidal surface. In another study carried out by Karabulut and Alnak (2020), heat transfer from copper plate surfaces with different patterns as rampart and rectangular was investigated using a single air jet stream in rectangular cross-section channels whose three sides are closed and one side is open, the distance between the jet and the

plate (H/D_h) is between 4-10. As a result of their research, they found a 31.45% higher mean Nu value on rectangular patterned surfaces compared to rampart patterned surfaces for the value where the Re is 4000 and the distance between the jet and the plate is 4. Nagesha et al. (2020) carried out experimental research on heat transfer from a single circular jet impinging on a flat plate with a protrusion of depths 1, 2 and 3 mm. Besides, they performed numerical simulations using ANSYS Fluent program to compare the results with those from experiments. Their results showed that the increase of jet Re and relative depth of protrusion enhances the heat transfer on the impinging surfaces up to 16.69% compared to a flat surface. In another work, round jet impingement on a heated flat plate at constant heat flux was analyzed experimentally and numerically by Issac et al. (2020). Experiments were done at various Re values ($Re_d=10000$ to 25000) and at four different nozzles to plate spacing ($h/d=4, 6, 8$ and, 10). However, $k-\omega$ SST, Realizable $k-\epsilon$, RNG $k-\epsilon$ and v^2f turbulence models were used to validate the numerical results with experimental results. They observed that the inlet turbulent intensity and eddy viscosity ratio are significant for the accurate prediction of realistic results. Huang et al. (2021) experimentally and numerically examined the heat transfer coefficients of a synthetic jet flow impingement onto the tip region of a longitudinal fin used in an electronics cooling system. The effects of different parameters, such as amplitude and frequency of diaphragm movement and jet-to-cooled-surface spacing were taken into consideration. Heat transfer coefficient values as high as $650 \text{ W/m}^2\text{K}$ were obtained with high-frequency diaphragm movement. Rathore and Verma (2022) performed numerical work about the effects of variation in Re and offset ratio (OR) on turbulent flow and thermal characteristics of oblique offset jet. Re and OR were considered in the range of $Re=10000-25000$ and $OR=3-11$. The obliquity angle of the offset jet range was taken as $90^\circ-45^\circ$ at an interval of 15° . They obtained that process of heat transfer from heated impingement wall to fluid is more intense for a higher value of jet obliquity angle and Re. Zou et al. (2022) used high-speed compressed air impinging to research the interfacial heat transfer and gas flow in the process of air-cooling in their experiment and numerical simulation. The effect of sample diameter and jet distance (distance from jet to cooling surface) on the flow pattern and temperature fields was studied. The results showed that smaller jet distances had a bigger interfacial heat transfer coefficient. Demircan (2019) numerically investigated the heat transfer from the electronic circuit element by cross-flow-impinging jet. Investigations were made at different values of Re and jet-channel velocity ratios. It was concluded that the heat transfer increased significantly with the improvement of Re and velocity ratios. Mergen (2014) investigated heat transfer by impinging jet-cross flow from an electronic element with a constant heat flux of 3500 W/m^2 . As a result, it was determined that the heat transfer decreased with the decrease of the jet

Re/channel Re (Re_j/Re_c) ratio. Heat transfer with impinging air jet-cross flow coexistence on a constant heat flux element was investigated numerically by Öztürk and Demircan (2022). In their study, the researchers investigated the heat transfer from a single element in the channel for different jet inlet velocity/channel inlet velocity ratios (0, 1, 2, and 3) and for different angles of the fins ($0^\circ, 22.5^\circ, 45^\circ, 67.5^\circ$ and 90°) placed in the duct, While the ratio of channel height to jet diameter was taken as constant and 3, the air was used as a fluid in the channel. It was determined that the highest heat transfer from the element was reached when the ratio of the inlet velocity to the channel inlet velocity was 3 and the fin angle was 90° . Maghrabie et al. (2017) numerically evaluated the heat transfer with the impinging jet-cross flow combination of a system consisting of seven circuit elements along the channel and determined the effect of the jet position change on the heat transfer.

When the jet impingement studies using nanofluids are examined, Chang and Yang (2014) studied the heat transfer performance of jet impingement flow boiling using Al_2O_3 -Water nanofluid. The heat transfer performance of the jet impingement flow of the Al_2O_3 -water nanofluid was found to be worse than the water used as the working fluid. It was determined that the decrease in heat transfer performance was due to the formation of a nano-absorption layer on the heated surface, which resulted in an increase in thermal resistance. However, while the formation of the nano-absorption layer is prevented by applying acoustic vibration to the heated surface, the heat transfer performance obtained using Al_2O_3 -Water nanofluid is better than that obtained using water. Datta et al. (2018) carried out a numerical simulation to investigate the heat transfer performance using Al_2O_3 -Water nanofluid in a confined slot jet impinging on a convex surface. In order to investigate the flow behaviour and convective heat transfer performance of the system, different parameters such as various Re values, and the distance between the jet and the plate were considered. They determined that the mean Nu and heat transfer coefficient increased significantly with the increase in the jet inlet Re. Kumar et al. (2021) used a heat sink combined with airfoil columns in the jet impingement condition to increase the heat transfer rate. While doing this, they used water and CuO -Water nanofluid with 1% concentration in their research. In their results, they found a 10% reduction in heat sink temperature when they used water fluid as a jet fluid, while the temperature drop was 14% when they used nanofluid. The flow of 0-6% Al_2O_3 -Water nanofluid in a microchannel with a serrated injection jet on the upper wall of the microchannel and using a magnetic field of 0-40 Hartman intensity was investigated by Jalali et al. (2022). The lower microchannel wall with the jet impingement chamber had a constant temperature, while the upper microchannel wall was insulated between the impinging jets. In order to increase heat transfer, the recessed mode

was applied for impinging jets. The results showed that when the notch height was high, the heat transfer was higher. Selimefendigil and Chamka (2020) aimed to numerically analyze the convection heat transfer properties in cooling an isothermal surface with a cavity-like part using a CuO-Water nano jet. They carried out their work by changing the volumetric concentration (0-4%) of the nanoparticle at different values of Re (100-400), different cavity lengths (5w-40w) and heights (w-5w). They found that when the cavity length is low, the contribution of the curved wall of the cavity to the mean Nu is significant and the mean heat transfer increases by 35-46% when nanofluid is used instead of water at the highest volumetric concentration. Abdullah et al. (2019) investigated the effect of TiO₂ nanofluid concentration on the heat transfer of double jet impinging on an aluminium plate surface by experimental analysis. Apart from this, the nozzle distance of the double jet and the nozzle-plate distance were considered as variables. Based on these data, they found that the flow structure of the double jet is an important condition affecting the heat transfer increase. In addition, they determined that the distances and nanoparticle concentration, which affect the flow structure, also affect the Nu together with the Re. Shi et al. (2021) experimentally investigated the effects of nano-aluminium additives on the instability of round water jets. Flow visualization in and near the exit of two transparent nozzles was obtained by high-speed shadow imaging technique and it was determined that the effects of nanoparticle additives on jet instability were mainly caused by viscosity increase and cavitation promotion.

As can be seen from the literature investigations, there are many studies with impinging jets. Although the number of combined jet flow studies in which the impinging jet and cross-flow are applied together using nanofluids is quite low, the study using GO-Water and Diamond-Water nanofluids, which exhibit high heat transfer performance at low concentrations, has not been found in the literature. In this study, heat transfer from two different model surfaces of roof and crown and flow structure in combined jet flow channels with H=3D height were numerically analyzed using water, 0.02% GO-Water and 2% Diamond-Water nanofluids without fin and with a fin at 90° angle at N=1.5D and 2D fin distances from the impinging jet inlet. The reason why the elements in the channel were chosen as different model surfaces is to increase the contact of the combined jet flow on the patterned surfaces to be cooled and it is to increase the heat transfer effect by ensuring that the jet flow is directed towards the other pattern in the channel after hitting a patterned surface. Considering the study conducted by Öztürk and Demircan (2022) in literature; the fin was positioned in such a way that it does not hinder the flow so that the cross-flow coming from the channel can be better directed on the models in the first row and the velocity of the fluid in the space between the models can be increased. Numerical research was carried out by solving steady and three-

dimensional energy and Navier-Stokes equations using the Ansys-Fluent program with the k-ε turbulence model. While the lower and upper surfaces of the fin and channel are adiabatic, the model surfaces have a constant heat flux of 1000 W/m², which is also applied in the literature (Shi et al., 2021; Kilic et al., 2017; Karabulut, 2019; Alnak et al., 2021). As it is known, overheating occurs under the intense working load of electronic elements. With this heat load, the temperatures of the elements can reach temperatures ranging from 308 to 353 K. In this study, the range of surface temperatures obtained for the roof and crown models is 303.4-307.2 K and 303.2-306.6 K, respectively. Therefore, it is seen that the constant heat flux approach of 1000 W/m² applied to the surfaces is correct. The Re range studied for fluids is 5000-15000. These selected Re values have been chosen based on the studies in the literature and represent both the jet Re (Re_j) and the channel Re (Re_c). Accordingly, in the study H=3D channel height, for GO-Water nanofluid flow in the jet and channel, the flow rates are V_j=0.355 m/s and V_c=0.103 m/s at values where the Re is 5000, respectively. For Re=15000, these values are V_j=1.064 m/s and V_c=0.310 m/s, respectively. Therefore, considering the studies reached in the literature, the Re range (Re=5000-15000) studied for both jet and channel flow is accepted as turbulent. The thermal conductivity, density and viscosity of the 0.02% volumetric concentration GO-Water nanofluid used in the study were obtained experimentally and only the specific heat was found with the help of the analytical model in the literature proposed by Pak and Cho (1998) by using the mixture rule of the base fluid and nanoparticle. However, the thermophysical properties of Diamond-Water nanofluid with 2% volumetric concentration were found with the help of the equations found in the literature. In addition to this, analyzes were carried out with the assumption that the nanofluid is a single-phase fluid. The results of the study were compared with the results of the equation obtained as a result of the experimental study in the literature and they were found to be compatible. The results were analyzed as the mean Nu and surface temperature variations for each roof and crown model surface in the channels. However, velocity and temperature contour distributions of the Diamond-Water nanofluid in finless and differentially spaced (N) finned channels for combined jet flow were presented for Re=11000. The mean Nu (Nu_m) and mean surface temperature (T_m) values were evaluated for all models found in the channels with Re=5000 and 15000 values in the finless and differentially spaced (N=1.5D and 2D) finned cases. In addition, the pressure drops of the fins and nanofluids compared to the Nu value increase in the combined jet flow channels according to the finless and water use cases were interpreted by considering the performance coefficient (C).

Preparation of GO-Water Nanofluid

The Graphene Oxide (GO) nanoparticle used in this study was synthesized from graphite. While synthesizing the GO nanoparticle, graphite was treated with various chemicals such as nitric and sulfuric acid as well as sodium nitrate, hydrogen peroxide and potassium permanganate. After these processes, graphite was passed through distilled water to separate it from acids and chemicals, and then oven-dried to obtain GO nanoparticles (Hajjar et al., 2014; Hummers and Offeman, 1958). GO-Water nanofluid was obtained with a two-stage nanofluid preparation method using the synthesized GO nanoparticle. The two-step procedure consists of mixing water with nanoparticles directly and passing it through an ultrasonicator device that generates ultrasonic sound waves to prevent the aggregation of nanoparticles in the resulting nanofluid. In addition, ultrasonic sound waves were used to mix the nanoparticles with the base fluid. GO nanoparticles were prepared by measuring with a precision balance with a precision of 0.1 mg, depending on the desired volumetric concentration. To obtain GO-Water nanofluid with 0.02% volumetric concentration, 0.8 g of GO nanoparticles were used. The obtained nanofluid was exposed to sound waves with an ultrasonicator device with a 50 Hz frequency and 230 W maximum power for 5 hours to ensure its stability. It was seen that the prepared nanofluid could preserve its stability without sedimentation for two months after being used in the experiments. Besides, it was decided that the stability of nanofluid was enabled in the result of the observation and Zeta potential measurements. While suspensions with high Zeta potential are in balance as electrical, suspensions with low Zeta potential tend to coagulate or aggregate. It is known that nanofluids with a Zeta potential between 40-60 mV have perfect stability. The Zeta potential value of the GO nanofluid used in the experiments is in the range of 45-65 mV, which is fairly higher than 25 mV which is the stability criteria value. In addition, an scanning electron microscope (SEM) image was exhibited to present the morphology of the experimentally obtained GO nanoparticle used in this study in Fig. 1 (Eravcu, 2016).

The volumetric nanoparticle concentration in the nanofluid is calculated by Eq. (1) (Karabulut et al., 2020).

$$\frac{v_p}{v_{nf}} = \frac{v_p}{v_{bf} + v_p} = \frac{\frac{m_p}{\rho_p}}{\frac{m_p}{\rho_p} + \frac{m_{bf}}{\rho_{bf}}} = \frac{m_p \rho_{bf}}{m_p \rho_{bf} + m_{bf} \rho_p} \quad (1)$$

In Equation (1), m_p and m_{bf} show the masses of nanoparticles and water, respectively, and ρ_{bf} and ρ_p

show the densities of water and nanoparticles, respectively.

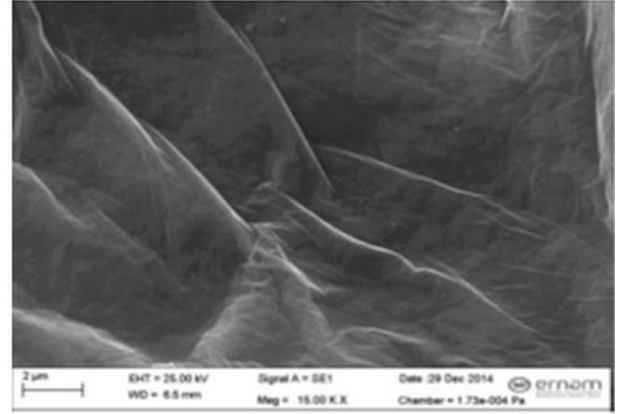


Figure 1. Image of GO obtained from the SEM (Eravcu, 2016)

Thermophysical Properties of GO-Water Nanofluid

While the viscosity value of the prepared nanofluid was measured with the Malvern Kinexus Pro cone and plate tension-controlled rheometer, the measurement of the thermal conductivity coefficient was carried out using the hot wire method, which is widely used in the literature, using the KD2 Pro thermal conductivity meter. Density measurements of the nanofluid were made experimentally with the Anton-Paar DMA 4200 Density Meter. Before the experimental thermophysical measurements of the GO-Water nanofluid used in the devices were carried out, measurements were made with water and the devices were calibrated. Then, the measurement values of the thermophysical properties of the nanofluid were taken after making more than one measurement and convincing the accuracy of it. However, the specific heat value of the nanofluid was obtained as a result of the analytical model proposed by Pak and Cho (1998) in Eq. (2).

$$c_{pnf} = (1 - \phi)c_{pbf} + \phi c_{pp} \quad (2)$$

In Equation (2), p , nf and bf denote particle, nanofluid and water fluid, respectively. In addition, due to the low concentration (0.02%), the specific heat value obtained as a result of the calculation of the nanofluid was taken as equal to water, since it is close to water.

Apart from the specific heat of GO-Water nanofluid and water, other thermophysical properties were obtained experimentally and are shown in Tab. 1 (Karabulut et al., 2020).

Uncertainty analyses of the measured values were obtained using Taylor (1997)'s uncertainty analysis method and were given in Tab. 2. The values shown are the maximum values for the given parameters, taking into account all experimental situations.

Table 1. Thermophysical properties of GO-Water and Water at 303 K

Fluid	k (W/mK)	ρ (kg/m ³)	c_p (J/kgK)	μ (Ns/m ²)
Water	0.6172	995.8	4178.4	803.4x10 ⁻⁶
GO-Water	0.678	996.1	4178.4	1060x10 ⁻⁶

Table 2. Results of uncertainty analysis for experimental values

Variable	Absolute uncertainty range	Unit
k	±0.006	W/mK
ρ	±9.9	kg/m ³
μ	±1.2x10 ⁻⁶	Ns/m ²
c_p	±41.78	J/kgK

Thermophysical Properties of Diamond-Water Nanofluid

Thermophysical properties of Diamond-Water nanofluid with 2% volumetric concentration, which is one of the working fluids used in this study, were obtained with the help of equations (Maxwell, 1873) found in the literature and widely used and shown in Tab. 3. In addition, the thermophysical properties of the solid diamond nanoparticle are also taken from the relevant study in the literature (Mohammed et al., 2011). The specific heat of the Diamond-Water nanofluid was calculated by Eq. (2).

The Eqs. (3, 4 and, 5) indicating density (ρ), thermal conductivity (k) and viscosity (μ) of the Diamond-Water Nanofluid are as follows (Maxwell, 1873; Mohammed et al., 2011).

The density of Diamond-Water Nanofluid

$$\rho_{nf} = (1 - \phi)\rho_{nf} + \phi\rho_p \quad (3)$$

Thermal Conductivity of Diamond-Water Nanofluid

$$k_{nf} = \frac{k_p + 2k_{bf} + 2(k_p - k_{bf})\phi}{k_p + 2k_{bf} - 2(k_p - k_{bf})\phi} k_{bf} \quad (4)$$

The viscosity of Diamond-Water Nanofluid

$$\mu_{nf} = \mu_{bf} (1 + 2.5\phi) \quad (5)$$

Table 3. Thermophysical properties of Water, Diamond-Water and, Diamond at 303 K

Properties	Water	Diamond-Water Nanofluid	Diamond
k (W/mK)	0.6172	0.6685	1000
ρ (kg/m ³)	995.8	1046.08	3510
c_p (J/kgK)	4178.4	4104.77	497.26
μ (Ns/m ²)	803.4x10 ⁻⁶	843.57x10 ⁻⁶	-

NUMERICAL METHOD

The Ansys-Fluent program was used to solve the forced convection heat transfer of the combined jet flow on the model surfaces.

Accurate modelling of turbulence is essential in heat transfer processes. However, direct numerical simulations of turbulent fluids are very difficult and also a time-consuming process. Although there are various turbulence models (Genç et al., 2009; Genç, 2010; Genç et al., 2011) used in numerical modelling, among these models in terms of being economical and yielding results with acceptable accuracy in many flow events; the k- ϵ turbulence model, which is a semi-empirical model, is widely used (Wang and Mujumdar, 2005). In one of the studies on impinging jets, Wang and Mujumdar (2005) tested several k- ϵ turbulence models with low Re values for turbulent jets. They found that the models were able to determine the general shape of the Nu distribution and that the models were better applied at the stagnation point for large jet-plate distances. In their study, they determined that the k- ϵ turbulence model performs well in determining the heat transfer properties of impinging jets when compared to the standard high Re models. In addition, they saw that the k- ϵ turbulence model is suitable as it approaches reducing the kinetic energy production and the result that should be in the stagnation region compared to other turbulence models in the study. Accordingly, considering the results obtained from the studies in the literature, the standard k- ϵ turbulence model was used for the channels in numerical calculations in this study.

Flow and heat transfer were done by solutions of differential equations derived from the equations of conservation of mass (continuity) (Eq. 6), momentum (Eq. 7) and energy (Eq. 8) for continuous, in which there is no body force, as follows (Wang and Mujumdar, 2005; Karabulut, 2019; Alnak et al., 2021).

Continuity equation

$$\frac{\partial \bar{u}_i}{\partial x_j} = 0 \quad (6)$$

Momentum equation

$$\rho \frac{\partial}{\partial x_j} (\bar{u}_i \bar{u}_j) = \frac{\partial \bar{P}}{\partial x_i} + \frac{\partial}{\partial x_j} \left[\mu \left(\frac{\partial \bar{u}_i}{\partial x_j} + \frac{\partial \bar{u}_j}{\partial x_i} \right) - \rho \overline{u'_i u'_j} \right] \quad (7)$$

Energy equation

$$\rho c_p \frac{\partial}{\partial x_i} (\bar{u}_i \bar{T}) = \frac{\partial}{\partial x_i} \left[k \frac{\partial \bar{T}}{\partial x_i} - \rho c_p \overline{T' u'_i} \right] \quad (8)$$

Equations of turbulence kinetic energy and turbulence kinetic energy disappearance of turbulent flow due to combined jet flow in the channel are given in Eqs. 9 and 10, respectively.

Turbulence kinetic energy equation

$$\frac{\partial}{\partial x_i} (\rho k u_i) + \frac{\partial}{\partial y} (\rho k) = \frac{\partial}{\partial x_j} \left[\mu + \frac{\mu_t}{\sigma_k} \frac{\partial k}{\partial x_j} \right] + G_k - \rho \varepsilon \quad (9)$$

Turbulence kinetic energy disappearance equation

$$\frac{\partial}{\partial x_i} (\rho \varepsilon u_i) + \frac{\partial}{\partial y} (\rho \varepsilon) = \frac{\partial}{\partial x_j} \left[\left(\mu + \frac{\mu_t}{\sigma_\varepsilon} \right) \frac{\partial \varepsilon}{\partial x_j} \right] + C_{1\varepsilon} \frac{\varepsilon}{k} G_k - C_{2\varepsilon} \rho \frac{\varepsilon^2}{k} \quad (10)$$

In these equations, ρ is the density of the fluid, k is the kinetic energy of the turbulent flow, u_i is the velocity components in the x , y and z directions, μ is the viscosity of the fluid, σ_k ($\sigma_k=1$) is the turbulent kinetic energy Pr. The equations showing turbulence kinetic energy production (G_k) and turbulent viscosity (μ_t) are as follows (Alnak et al., 2021; Genç et al., 2009).

$$G_k = -\rho \overline{u'_i u'_j} \frac{\partial u_j}{\partial x_i} \quad (11)$$

$$\mu_t = C_\mu \rho \frac{k^2}{\varepsilon} \quad (12)$$

The turbulence disappearance Pr is denoted by σ_ε , while $C_{1\varepsilon}=1.44$, $C_{2\varepsilon}=1.92$, $C_\mu=0.09$, and $\sigma_\varepsilon=1.3$ are coefficients in the equations (Saleha et al., 2015).

Heat transfer coefficient h and Nu are calculated with Eqs. 13 and 14, respectively (Incropera et al., 2007).

$$h = \frac{q''}{T_s - T_a} \quad (13)$$

Nu value

$$-k_f \left(\frac{\partial T}{\partial n} \right)_s = h(T_a - T_s) \text{ and } Nu = \frac{h(3m)}{k_a} \quad (14)$$

In these equations, T_a and T_s are the mean surface temperatures of the fluid and the model (K), respectively, k_f is the thermal conductivity of the fluid (W/m.K), $3m$ is the total surface length of the model with which the fluid is in contact (m), and h and h_m are the point and mean convective heat transfer coefficient (W/m².K) along the model surface, respectively, where n is the direction perpendicular to the surface. The model surface mean heat transfer coefficient and Nu value (Nu_m) are found in Eqs. 15 and 16 as given below, respectively.

Model surface mean heat transfer coefficient

$$h_m = \frac{1}{3m} \int_0^{3m} h dx \quad (15)$$

Model surface mean Nu value

$$Nu_m = \frac{h_m(3m)}{k_f} \quad (16)$$

Eq. 17 showing the hydraulic diameter of the channel is as follows.

$$D_{ch} = \frac{4A_c}{P_c} = \frac{4(H.W)}{2(H+W)} \quad (17)$$

In this equation, A_c and P_c represent the cross-sectional area and perimeter of the channel, respectively, while the height and width of the channel are represented by H and W . Jet inlet diameter D is equal to circular inlet jet hydraulic diameter D_{chjet} .

The Re values of the channel and the jet are determined using Eqs. (18) and (19).

$$Re_c = \frac{\rho V_c D_{ch}}{\mu} \quad (18)$$

$$Re_j = \frac{\rho V_j D_j}{\mu} \quad (19)$$

In these equations, the channel and jet flow velocities of the fluid are denoted by V_c and V_j (m/s), respectively.

The pressure drop (ΔP) is calculated by the following Eq. (20)

$$\Delta P = \frac{f \rho L}{2D_{ch}} V_c^2 \quad (20)$$

In this equation, ΔP represents the pressure drop (Pa) between the inlets and outlets of finless and finned ducts, f represents the friction factor, and L represents the length of the duct (m).

The coefficient of performance (C) is found in the following Eq. (21) (Alnak, 2020).

$$C = \frac{(Nu_{m-finned} / Nu_{m-finless})}{(\Delta P_{finned} / \Delta P_{finless})} \quad (21)$$

MODEL GEOMETRIES

While the dimensions of the impinging jet-cross flow combined jet flow finned channels and the models with roof and crown surfaces and fin geometry in the channels are given in Figs. 2 (a), (b), and (c), the dimensions of the channels are given in Tab. 4 (Öztürk and Demircan, 2022). During all tests, there are three models in each channel. The “Without fin” case refers to channels with models but no fin. The fin with 90° angle was placed in the channel as one at $N=1.5D$ and $N=2D$ distances from the impinging jet inlet towards the cross-flow channel entrance. In addition, the regular tetrahedral mesh structure used in the numerical

calculations of the combined jet flow channels is shown in Fig. 3.

In addition, the assumptions and boundary conditions made in this study are as follows. (a) Steady, three-dimensional and turbulent flow volumes were used, (b) Water, 0.02% GO-Water and 2% Diamond-Water nanofluids used as incompressible fluids were both jet and cross-flow fluids, (c) The thermal properties of the fluids are constant and independent of temperature, (d) The surfaces of the channel and the fin are adiabatic, (e) There is no heat source on water, nanofluid and patterned surfaces, (f) The outlet pressure of the duct was taken as equal to the atmospheric pressure ($P_o=P_{atm}$), (g) It was determined as $\partial T/\partial x=0$ assuming that the temperature difference at the exit of the channel was negligible, (h) It is assumed that there is a non-slip boundary condition on the channel, fin and pattern surfaces, and therefore, all velocity component values on the mentioned surfaces are zero.

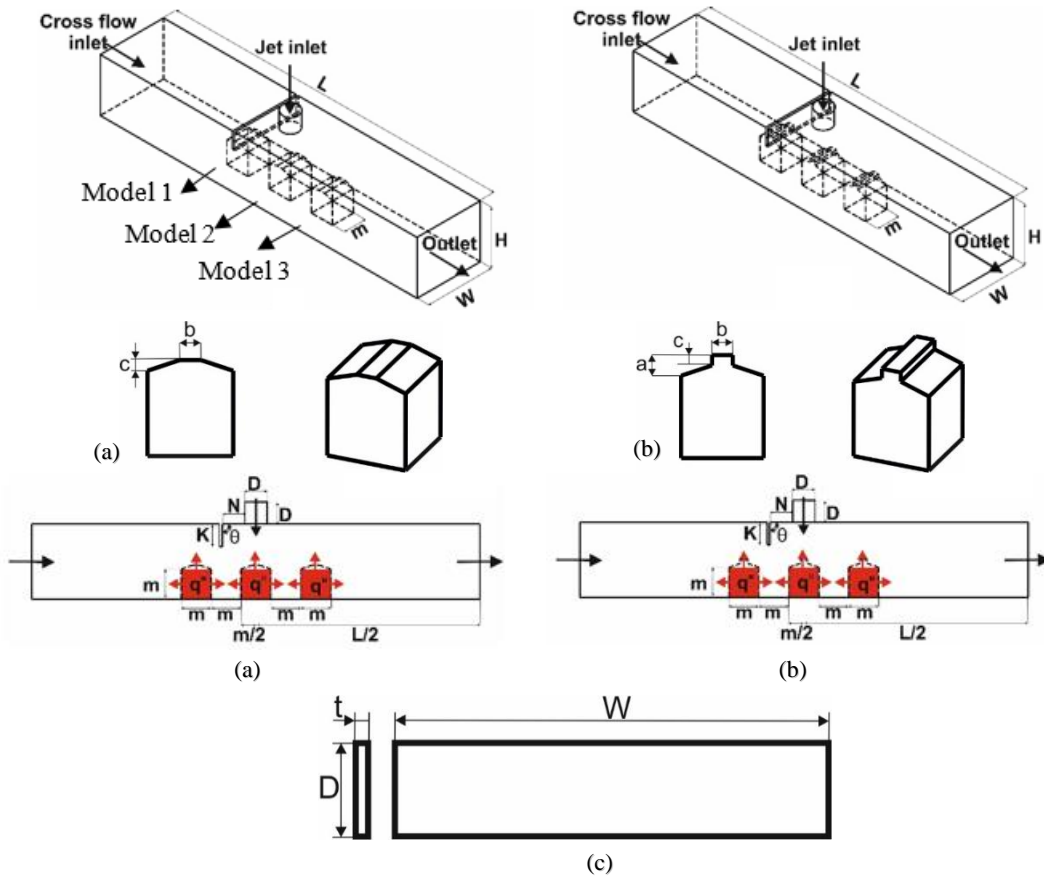


Figure 2. Views of channels with (a) Roof (b) Crown model surfaces (c) fin geometry

Table 4. Dimensions of the channels

Variable	Measurement
D	15 mm
L	66D
W	4D
H	3D
M	20 mm
θ	90°
N	1.5D, 2D
a	5 mm
b	5 mm
c	2.5 mm
t	0.1 mm

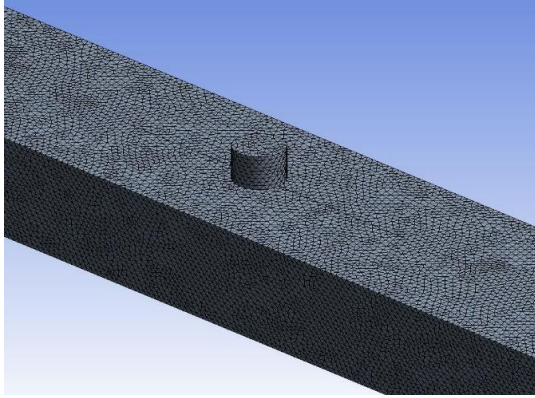


Figure 3. Representation of the regular tetrahedral mesh structure used in the channel

FINDINGS AND DISCUSSION

In the study, shown in Fig. 4, the results obtained by examining different Re values in the case of only jet flow and by using the equation ($\overline{Nu} = 1.29 Re^{0.5} Pr^{0.4}$) as a result of the experimental investigations of Ma and Bergles (1983) were compared among themselves, and it was determined that the experimental results of Ma and Bergles (1983) and the numerical results of the presented study were compatible and consistent.

In addition, the numerical results of this study were compared with the experimental study of the turbulent flow around a cube exposed to cross flow and impinging jet combined flow by Masip et al. (2012) and it was pointed out in Fig. 5. Masip et al. (2012) placed a cube-shaped model in a 2000x300x30mm channel in their study. Assuming that all surfaces of the channel were taken adiabatically, by taking the ratio of the jet Re (Re_j) to the channel Re (Re_c) equal ($Re_j/Re_c=1$), the flow structures around the electronic model were investigated at different positions (x/h). As can be seen in Fig. 5, it was determined that the velocity profiles obtained as a result of the experimental study conducted by Masip et al. (2012) were quite compatible with each other.

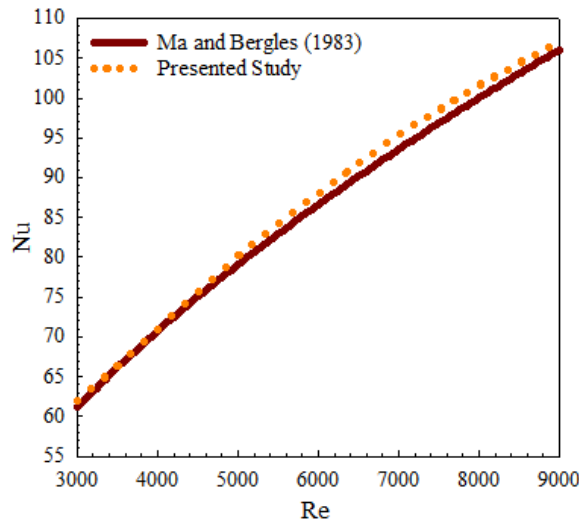


Figure 4. Comparison of the presented study and the results of Ma and Bergles (1983)

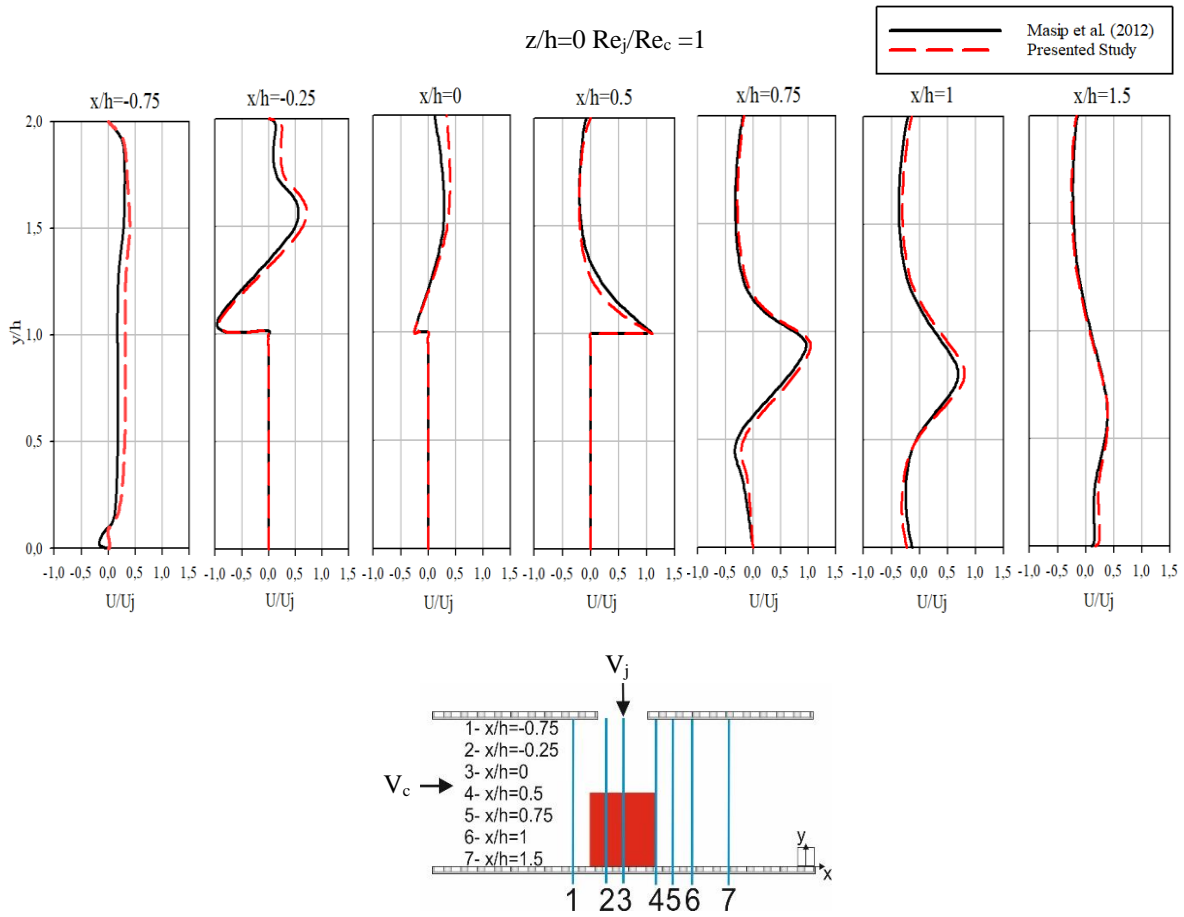


Figure 5. Comparison of the presented study and the results of Masip et al. (2012)

Provided that the variation of Nu depending on the mesh number was determined; by determining the most suitable number of mesh elements in the channel, the effect of mesh number on the mean Nu value (Nu_m) in

the finless combined jet flow channel was presented in Tab. 5 at different Re values. Accordingly, it was found that 2022840 mesh elements will give reliable and accurate results for the finless channel.

Table 5. Variation of Nu_m with Re depending on the number of mesh elements

Mesh number	$Re=5000$ Nu_m	$Re=7000$ Nu_m	$Re=9000$ Nu_m
1758412	86.48	108.84	127.40
2022840	86.52	108.88	127.43
2245786	86.52	108.87	127.42

The mean Nu value variations of roof and crown model surfaces according to model rows in channels having combined jet flow without fin and with 90° angled fin at $1.5D$ and $2D$ distance (N) by using Water, 0.02% GO-Water and, 2% Diamond-Water nanofluids are shown in Figs. 6 and 7, respectively. As the nanofluids in the combined jet flow channels contain GO and Diamond nanoparticles with a higher thermal conductivity coefficient in nano size (10^{-9} m) for both patterned model surfaces, the Nu value is higher than the channels in which only water is used, which means an increase in heat transfer from the surfaces to the nanofluid. While the Nu values are higher in the channel in which GO-Water nanofluid is used for both roof and crown model surfaces and fin distances ($N=1.5D$ and $2D$) in the first row (Model 1), compared to the channels in which

Diamond-Water nanofluid is used, the Nu values depending on Re are higher in finned channels compared to roof patterned surfaces for the crown patterned surfaces. In addition, Nu values are higher for all pattern rows, water and for both nanofluids as a result of better mobility for the roof model surfaces in the case of the finless channels compared to the crown model surfaces. While the mean Nu value for the Model 1 surface with roof at $Re=11000$ is 10.24% higher for the GO-Water nanofluid in the case with $N=2D$ fin distance than $N=1.5D$, this increment value is 26.82% for the crown model surface. As can be seen, when the fin is moved away from the jet inlet, the cooling of the surfaces improves as the cross flow is better directed on the surfaces and contributes additionally to the impinging jet flow. When the Model 2 surfaces, which are in the second row in the channels, are examined, it is

seen that the highest Nu values are reached in the channels with $N=2D$ fin distance in both models for this model row, which is under the influence of the directly impinging jet. In addition, Nu values in this model row, where the combined jet effect is the most intense, are higher than both Model 1 and Model 3. In the case where the Re is 15000 for the $N=2D$ fin position in the channels in which the Diamond-Water nanofluid is used, the value of mean Nu of the second-row surface with the crown model (Model 2) is 17.9% higher than the surface with the roof model in the same row. Model 3, located at the end of the channel, has the least combined jet effect for both model surfaces. Therefore, Nu values show a decrease for this model row (Model 3) especially compared to Model 2. When GO-Water nanofluid is used in channels with $N=1.5D$ fin distance at $Re=7000$, compared to channels without fins and water fluid is used, the mean Nu increase values in Model 3 compared to Model 2 on crown and roof model surfaces are found to be 53.76% and 36.34% less, respectively.

According to the placement rows of the roof and crown model surfaces in the channel without a fin and, with $N=1.5D$ and $N=2D$ fin distance by using Water, 0.02% GO-Water and 2% Diamond-Water nanofluids, the mean temperature variations on the model surfaces are given depending on the Re in Figs. 8 and 9, respectively. With the increase of Re in all model rows for both model surfaces, the heat transfer from the surfaces increases with the mobility of the fluid in the combined jet flow channels. Accordingly, the temperature of the model surfaces decreases. However, when the fin is added to the channel and especially in the $N=2D$ fin distance with GO-Water nanofluid, while the cooling of the surfaces is at the best level compared to the finless condition for all model rows and both model shapes; lower surface temperature values can be obtained on the crown model surfaces than that of the roof model. Since Model 2 is under the direct impact of the impinging jet, the combined jet effect increases on the model surface, and the surface temperature values decrease on both model-shaped surfaces compared to Model 1. Besides, while the cooling effect is better in finned channels, for the $N=2D$ distance where nanofluids are used, more reduction in surface temperatures is provided due to the increase in heat transfer on both model surfaces. When Model 3, which is in the third row in the channels, is examined, the decrease in the combined jet flow intensity in the models in this row for both model surfaces causes the surface temperatures to increase compared to Model 2 and depending on the model shape. Better orientation of the combined jet flow towards Model 3 after hitting Model 2 ensures that the surface temperature is lower for the crown model surface than that of the roof model.

C (Performance Coefficient) in the combined jet flow channels using Water, 0.02% GO-Water and, 2% Diamond-Water nanofluids belonging to the roof and crown model surfaces are shown according to different

fin placement distances ($N=1.5D$ and $2D$) in Figs. 10 and 11, respectively. For both model surfaces, higher C coefficient values are obtained in channels with $N=1.5D$ fin distance and Diamond-Water nanofluid than in channels with $N=2D$ fin distance using GO-Water nanofluid and Water. This situation is caused by the less pressure drop of the Diamond-Water nanofluid compared to the GO-Water nanofluid, while the fact that the fin makes difficult of the flow passage in the $N=2D$ position is another factor that increases the pressure drop compared to the $N=1.5D$ position. Therefore, although the Nu values are higher for the $2D$ distance, the C values obtained for the $1.5D$ fin distance are higher than the $2D$ distance due to the low-pressure losses. For $N=1.5D$ at $Re=11000$, the C value obtained for the Diamond-Water nanofluid on the crown model surface is 6.05% higher than the roof model surface. However, as the pressure drop increases with the increase in the Re, the C values also decrease. Besides, the fact that the C is more than 1 indicates that the use of a fin has an increasing effect on heat transfer despite the pressure drop.

Mean Nu (Nu_m) and surface temperature (T_m) values for all three roof and crown model surfaces in the combined jet flow channels at Re values of 5000 and 15000 are given in Tab. 6 for without fin and with fin and, $N=1.5D$ and $N=2D$ fin distance, respectively. In the case of using fins in both model surface channels, Nu_m values increase while T_m values decrease. However, when nanofluid is used, higher Nu_m values are obtained due to the increase in heat transfer from the model surfaces compared to the water fluid, while the mean surface temperature values (T_m) decrease with the cooling effect. In addition, the highest Nu_m values are reached on the crown patterned surfaces with fins at $N=2D$ distance and using GO-Water nanofluid compared to the $N=1.5D$ fin distance and the use of Diamond-Water nanofluid. Nu_m increases for GO-Water nanofluid at $Re=15000$ and $N=2D$ fin distance according to $N=1.5D$ are 7.24% and 16.38% compared to the case of using finless and water fluid for roof and crown models, respectively. Accordingly, lower T_m values are obtained in the channels with crown model surfaces compared to channels with roof surfaces. Besides, Nu_m increases for GO-Water and Diamond-Water nanofluids at $Re=15000$ and $N=2D$ are 47.53%-46.21% and 57.42%-56.18% compared to the case of using finless and water fluid for roof and crown models, respectively.

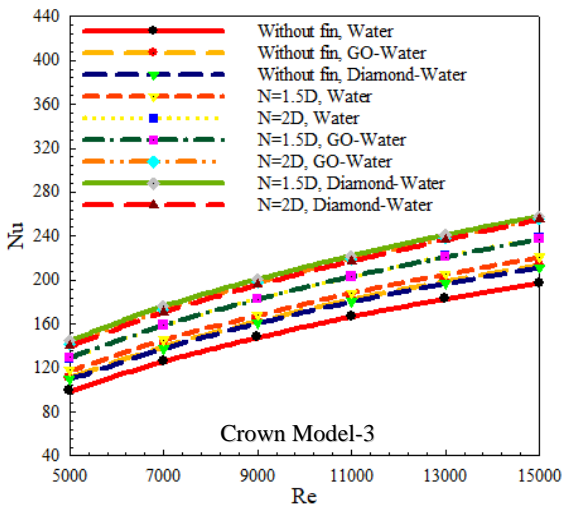
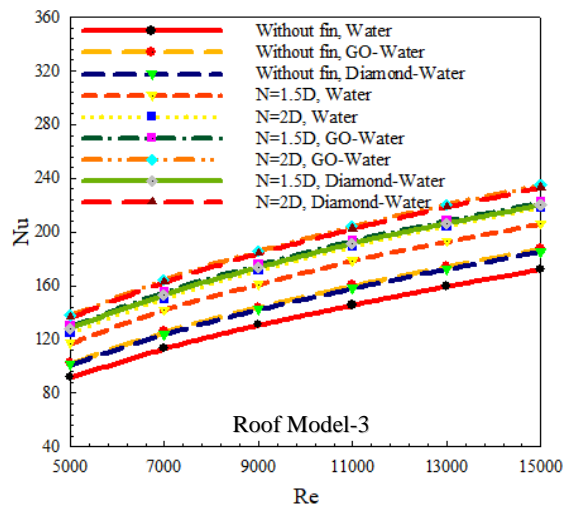
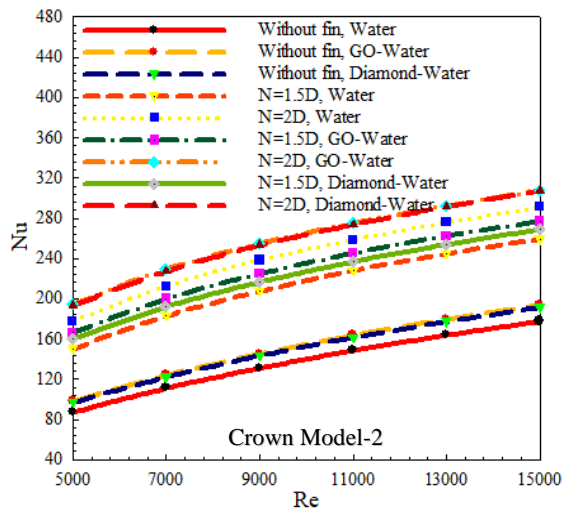
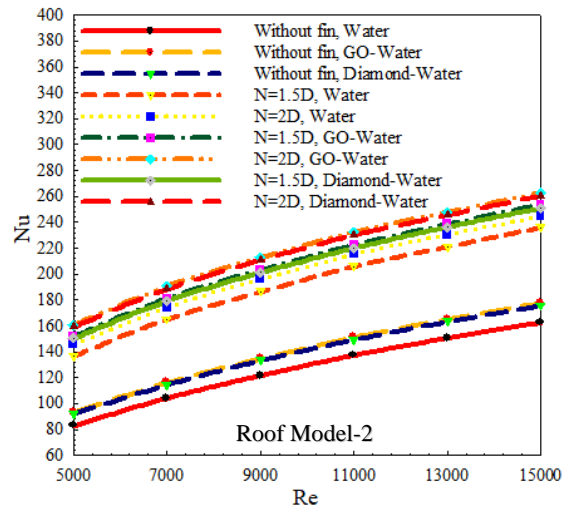
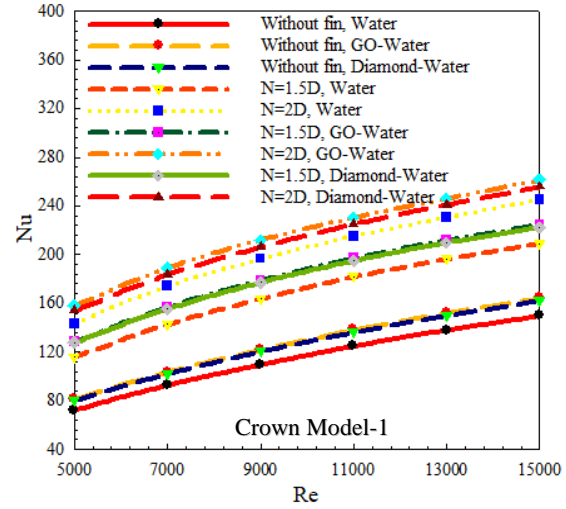
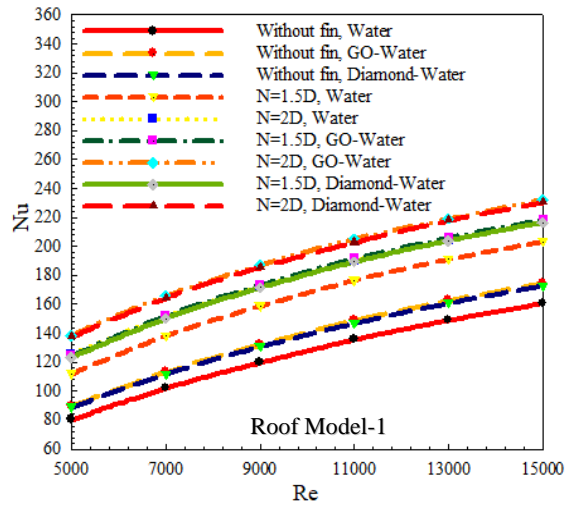


Figure 6. Variation of mean Nu value with Re according to model rows in cross flow-impinging jet flow channels with roof model

Figure 7. Variation of mean Nu value with Re according to model rows in cross flow-impinging jet flow channels with crown model

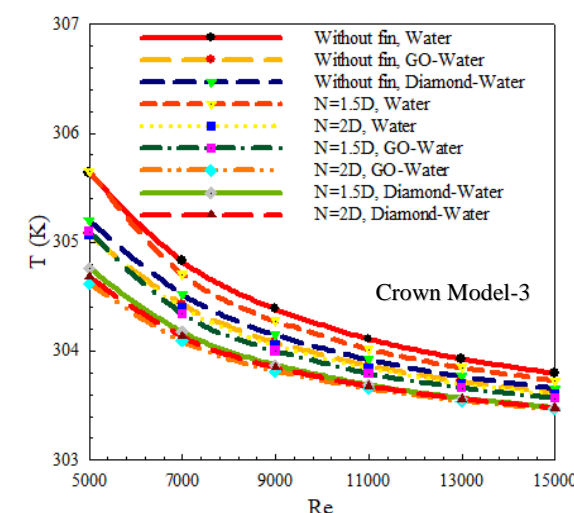
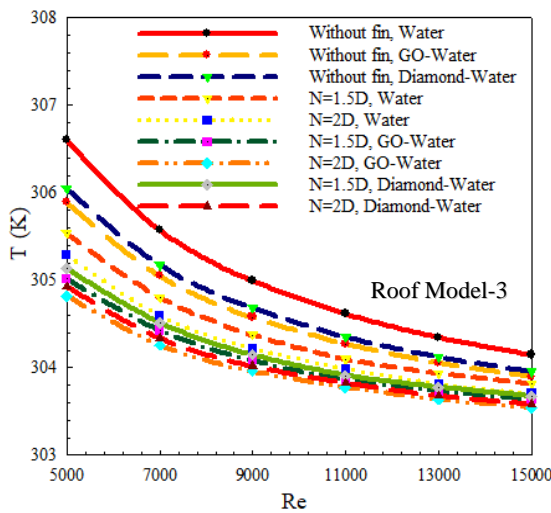
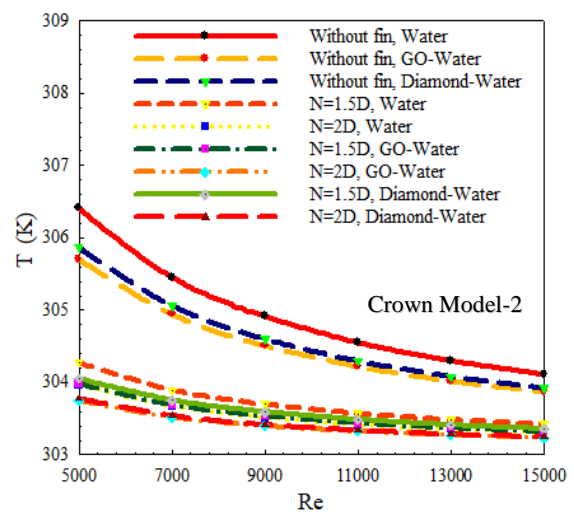
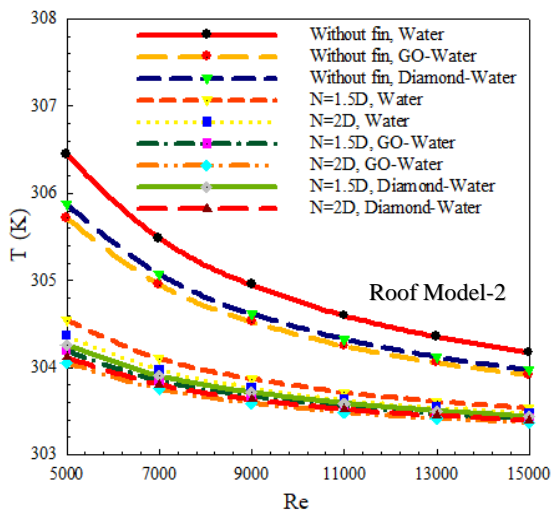
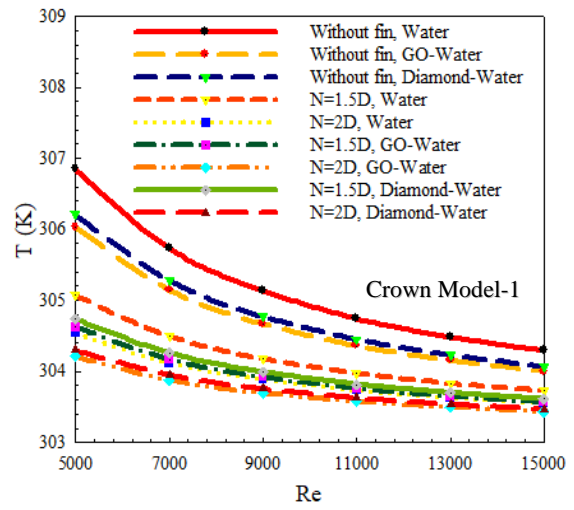
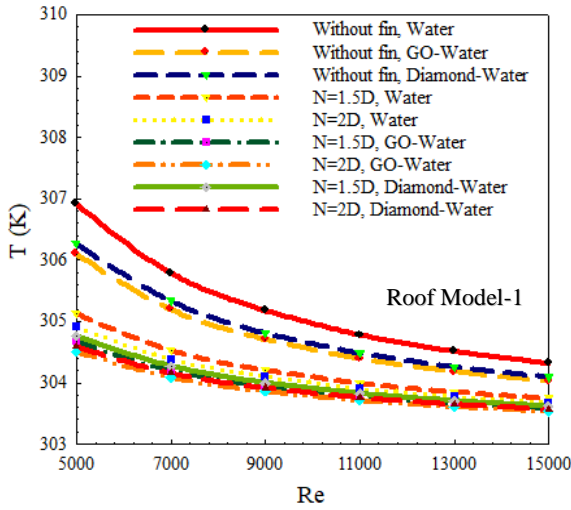


Figure 8. Variation of mean surface temperature (T) with Re according to model rows in cross flow-impinging jet flow channels with roof model

Figure 9. Variation of mean surface temperature (T) with Re according to model rows in cross flow-impinging jet flow channels with crown model

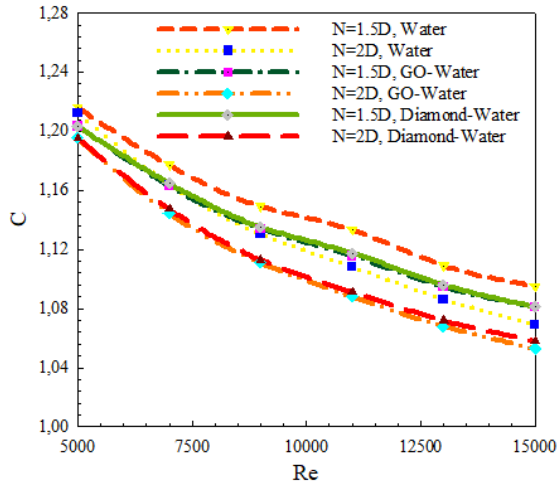


Figure 10. Variation of C with Re for $N=1.5D$ and $N=2D$ in cross-flow-impinging jet-flow channels with roof model

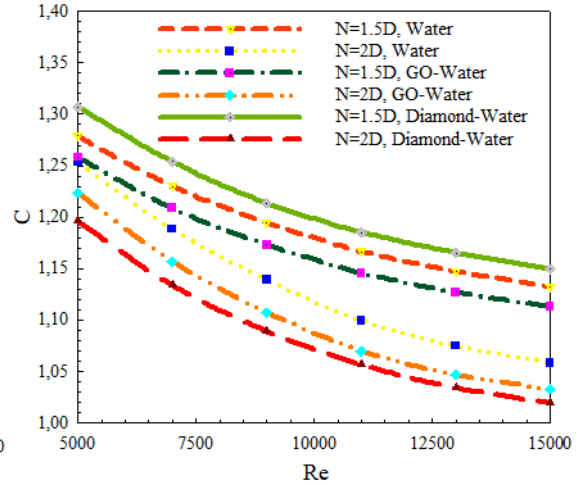


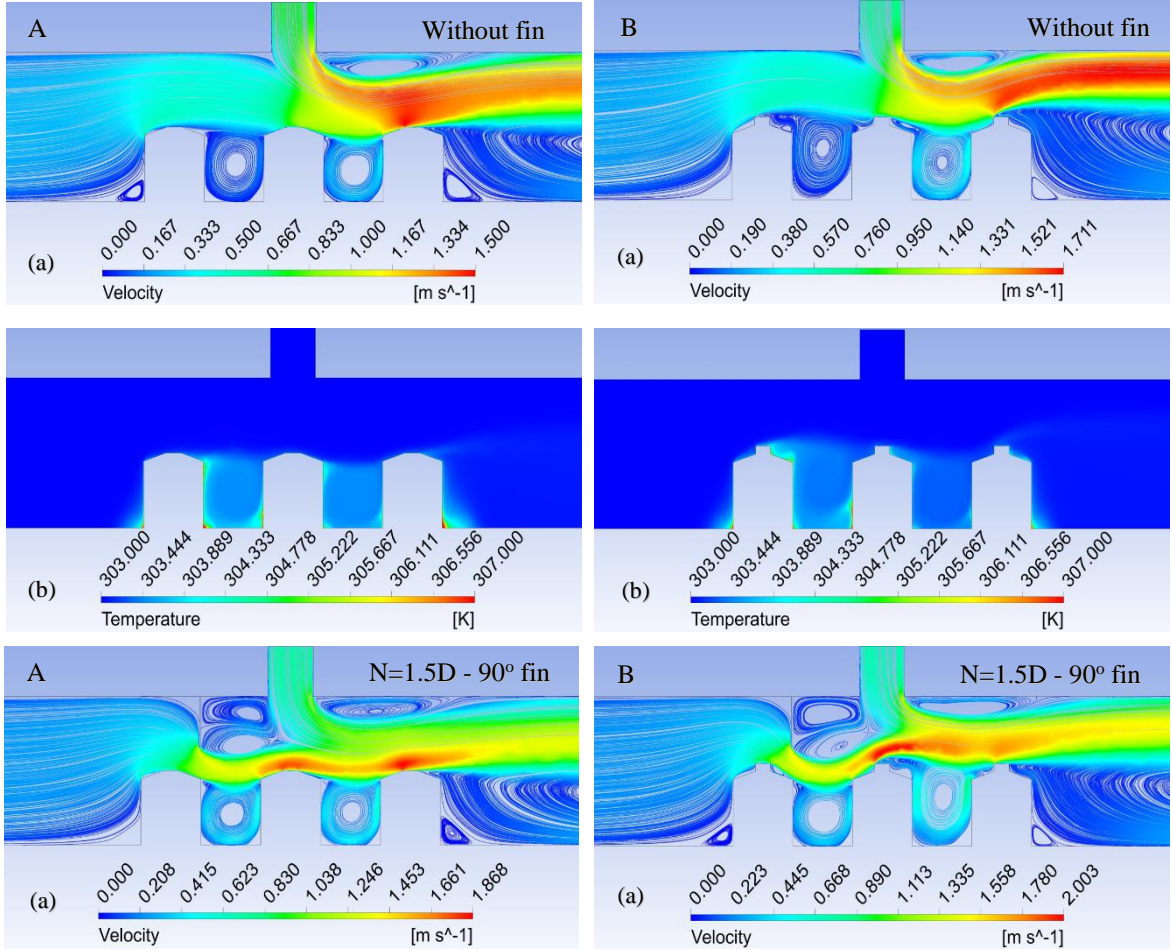
Figure 11. Variation of C with Re for $N=1.5D$ and $N=2D$ in cross-flow-impinging jet-flow channels with crown model

In Fig. 12 A-Roof Model and B-Crown Model, (a) velocity and (b) temperature contour distributions are presented in the combined jet flow channels without fin and, with 90° angled fin having $N=1.5D$ and $2D$ distance by using Diamond-Water nanofluid at $Re=11000$, respectively. As can be seen from the velocity contour distributions, the velocity values on Model 1 are lower since Model 1 is mostly under the influence of the cross-flow coming from the channel inlet in the finless condition in both model-surfaced channels. Although there is an impinging jet flow on Model 2, the cross-flow drags this flow towards Model 3, increasing the combined jet flow velocity on this model without fin. For this reason, although Model 3 is at the end of the channel, the cooling performance is close to Model 2 under the impact of the impinging jet, as can be seen from the temperature distributions for both model shapes, in the finless condition. This is also contributed by the recirculation zones on the upper right side of the

impinging jet flows in the channels to direct the combined jet flow towards Model 3. When fins are added to the channels ($\theta=90^\circ$), since the cross-flow from the channel can be directed on the model surfaces, the contact of the fluid with the surface increases, at the same time, a jet flow effect occurs on the surfaces due to the decrease in the flow passage cross-sectional area. When the fin is placed at a distance of $N=1.5D$ from the channel, the combined jet flow effect of the fluid shows itself with velocity increases on all models and for both model shapes; in $N=2D$ fin position, the velocity of the fluid on Model 3 decreases as the fluid hits the upper part of Model 2 and is directed to the upper part of the channel for Model 3 with the crown pattern. Besides, with the use of fins, the heat transfer from the model surfaces is increased by providing the movement of the fluid located between the models and circulating in itself, which contributes negatively to the cooling of the models.

Table 6. Analysis results of Nu_m and T_m values for all three roof and crown model surfaces in cross-flow-impinging jet channels with Water, GO-Water and, Diamond-Water nanofluid

			Re=5000		Re=15000	
			Roof Model	Crown Model	Roof Model	Crown Model
Without fin	Water	Nu_m	84.891	86.197	164.991	174.560
Without fin	GO-Water	Nu_m	95.098	96.865	179.896	190.352
Without fin	Diamond-Water	Nu_m	94.042	95.74	177.944	188.281
N=1.5D	Water	Nu_m	122.028	127.987	215.094	229.679
N=2D	Water	Nu_m	131.943	150.110	226.793	258.162
N=1.5D	GO-Water	Nu_m	135.338	141.486	231.474	246.209
N=2D	GO-Water	Nu_m	145.735	164.749	243.420	274.793
N=1.5D	Diamond-Water	Nu_m	134.024	144.407	229.090	249.710
N=2D	Diamond-Water	Nu_m	144.409	162.347	241.246	272.638
Without fin	Water	T_m (K)	306.652	306.297	304.208	304.062
Without fin	GO-Water	T_m (K)	305.900	305.606	303.943	303.827
Without fin	Diamond-Water	T_m (K)	306.061	305.755	304.003	303.880
N=1.5D	Water	T_m (K)	305.067	304.998	303.695	303.624
N=2D	Water	T_m (K)	304.857	304.523	303.618	303.487
N=1.5D	GO-Water	T_m (K)	304.627	304.570	303.541	303.485
N=2D	GO-Water	T_m (K)	304.460	304.192	303.481	303.378
N=1.5D	Diamond-Water	T_m (K)	304.719	304.516	303.576	303.483
N=2D	Diamond-Water	T_m (K)	304.542	304.250	303.512	303.395



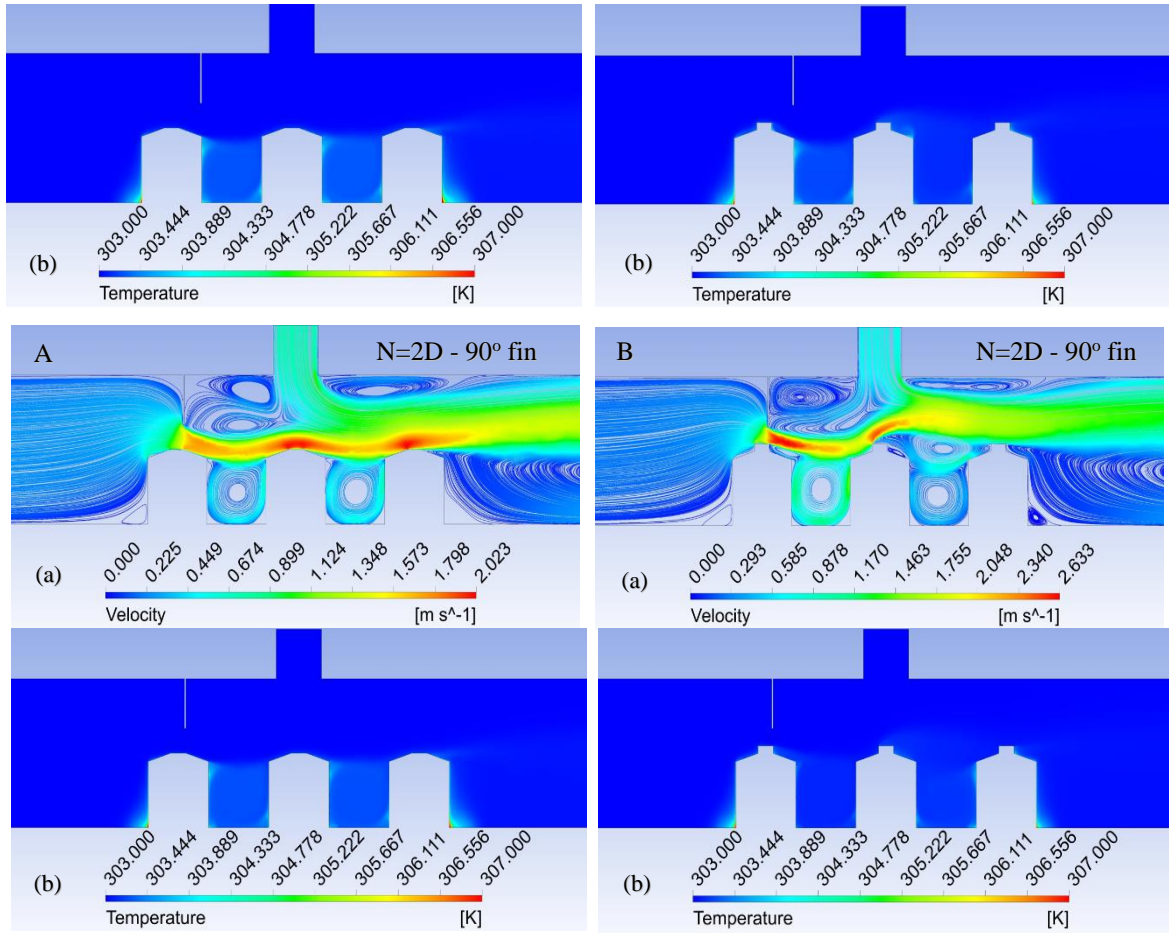


Figure 12. (a) Velocity (b) Temperature contour distributions in cross flow-impinging jet flow channels with A-Roof B-Crown model for Diamond-Water nanofluid

CONCLUSIONS

In this study, the heat transfer and flow structure from the roof and crown model surfaces in the combined jet flow channels with $H=3D$ height by using cross flow-impinging jet flow were numerically analyzed without fin and with fin angle of 90° and, fin arranged from the impinging jet inlet as $N=1.5D$ and $N=2D$ distances. While a constant heat flux of 1000 W/m^2 was applied to the model surfaces, Water, GO-Water and Diamond-Water nanofluids with a volumetric concentration of 0.02% and 2%, respectively, were used as fluids in the channels. As a result of this numerical study, in which a detailed examination of the cross-flow-impinging jet flow using different nanofluids was made, the following results can be reached.

- Nu values are higher for all pattern rows, water and for both nanofluids for the roof model surfaces in the case of the finless channels compared to the crown model surfaces.

- While the Nu values are higher in the channel in which GO-Water nanofluid is used for the roof and crown model surfaces and fin distances ($N=1.5D$ and $2D$) in the first row (Model 1), compared to the channels in

which Diamond-Water nanofluid is used, the Nu values depending on Re are higher in finned channels compared to roof model surfaces for the crown model.

- While the mean Nu value for the Model 1 surface with roof at $Re=11000$ is 10.24% higher for the GO-Water nanofluid in the case with $N=2D$ fin distance than $N=1.5D$, this increment value is 26.82% for the crown model surface.

- At $Re=15000$ for the $N=2D$ fin position in the channels in which the Diamond-Water nanofluid is used, the mean Nu value of the crown model (Model 2) is 17.9% higher than the surface with the roof Model 2.

- When the GO-Water nanofluid is used in channels with $N=1.5D$ fin distance at $Re=7000$, compared to channels without fins and water fluid is used, the mean Nu increase values in Model 3 compared to Model 2 on crown and roof model surfaces are found to be 53.76% and 36.34% less, respectively.

- The highest Nu_m values are reached on the crown patterned surfaces with a fin at $N=2D$ distance and using

GO-Water nanofluid compared to the $N=1.5D$ fin distance and the use of Diamond-Water nanofluid.

- Nu_m increases for GO-Water nanofluid at $Re=15000$ and $N=2D$ fin distance according to $N=1.5D$ are 7.24% and 16.38% compared to the case of using finless and water fluid for roof and crown models, respectively. Accordingly, lower T_m values are obtained in the channels with crown model surfaces compared to channels with roof surfaces.

- Although the Nu values are higher for the $2D$ distance, the C values obtained for the $1.5D$ fin distance are higher than the $2D$ distance due to low-pressure losses.

- For $N=1.5D$ at $Re=11000$, the C value obtained for the Diamond-Water nanofluid on the crown model surface is 6.05% higher than the roof model surface. However, as the pressure drop increases with the increase in the Re , the C values also decrease.

As a result, increasing the heat transfer from the model surfaces in the combined jet flow channels is of great importance in terms of the operation of the circuit within safe temperature limits. In this case, apart from the model shape of the surfaces, the fin setup and fin placement used to direct the fluid in the channel to the model surfaces, the channel and jet Re values and the thermophysical properties of the fluid are the main factors.

ACKNOWLEDGMENTS

This study was supported by Sivas Cumhuriyet University Scientific Research Projects (CUBAP) unit with project number TEKNO-2021-031.

REFERENCES

Abdullah M. F., Zulkifli R., Harun Z., Abdullah S., Wan Ghopa W. A., Najm A. S., Sulaiman N. H., 2019, Impact of the TiO_2 Nano Solution Concentration on Heat Transfer Enhancement of the Twin Impingement Jet of A Heated Aluminium Plate, *Micromachines*, 10, 176.

Alnak D. E., Koca F., Alnak Y. A., 2021, Numerical Investigation of Heat Transfer from Heated Surfaces of Different Shapes, *J. Eng. Therm.*, 30, 494-507.

Alnak D. E., 2020, Thermohydraulic Performance Study of Different Square Baffle Angles in Cross-Corrugated Channel, *J. Energy Storage*, 28, 101295.

Chang T. B., Yang Y. K., 2014, Heat Transfer Performance of Jet Impingement Flow Boiling Using

Al_2O_3 -Water Nanofluid, *J. Mech. Sci. Technol.*, 28, 1559-1566.

Datta A., Jaiswal A., Halder P., 2018, Heat Transfer Analysis of Slot Jet Impingement Using Nano-Fluid on Convex Surface, *IOP Conf Series-Mat. Sci. Eng.*, 402, 012098.

Demircan T., 2019, Numerical Analysis of Cooling An Electronic Circuit Component with Cross Flow and Jet Combination, *J. Mech.*, 35, 395-404.

Eravcu F., 2016, *Synthesis, Characterization, Rheology, Thermal Conductivity and Stability of Carbon-Based Nanomaterials*, MSc. Thesis, Sivas Cumhuriyet University, Sivas, Turkey.

Genç M. S., Kaynak Ü., Yapıcı H., 2011, Performance of Transition Model for Predicting Low Re Aerofoil Flows without/with Single and Simultaneous Blowing and Suction, *Eur. J. Mech. B/Fluids*, 30, 218-235.

Genç M. S., 2010, Numerical Simulation of Flow Over A Thin Aerofoil at A High Reynolds Number Using A Transition Model, *Proc. Inst. Mech. Eng. Part C: J. Mech. Eng. Sci.*, 24, 2155-2164.

Genç M. S., Kaynak U., Lock G. D., 2009, Flow Over An Aerofoil without and with A Leading- Edge Slat at A Transitional Reynolds Number, *Proc. Inst. Mech. Eng. Part G: J. Aeros. Eng.*, 223, 217-231.

Hadipour A, Zargarabadi M. R., 2018, Heat Transfer and Flow Characteristics of Impinging Jet on A Concave Surface at Small Nozzle to Surface Distances, *Appl. Therm. Eng.*, 138, 534-541.

Hajjar Z., Rashidi A., Ghozatloo A., 2014, Enhanced Thermal Conductivities of Graphene Oxide Nanofluids, *Int. Commun. Heat Mass Transf.*, 57, 128-131.

Huang L., Yeom T., Simon T., Cui T., 2021, An Experimental and Numerical Study on Heat Transfer Enhancement of A Heat Sink Fin by Synthetic Jet Impingement, *Heat Mass Transf.*, 57, 583-593.

Hummers W. S., Offeman R. E., 1958, Preparation of Graphitic Oxide, *J. American Chem. Soc.*, 80, 1339.

Incropera F. P., Dewit D. P., Bergman T. L., Lavine A. S., 2007, *Fundamentals of Heat and Mass Transfer*, 6th Ed. In: John Wiley&Sons, United States of America.

Issac J., Singh D., Kango S., 2020, Experimental and Numerical Investigation Of Heat Transfer

- Characteristics of Jet Impingement on A Flat Plate, *Heat Mass Transf*, 56, 531-546.
- Jalali E., Sajadi S. M., Ghaemi F., Baleanu D., 2022, Numerical Analysis of the Effect of Hot Dent Infusion Jet on the Fluid Flow and Heat Transfer Rate Through the Microchannel in the Presence of External Magnetic Field, *J. Therm. Anal. Calorim.*, 147, 8397-8409.
- Karabulut K., Alnak D. E., 2021, Investigation of the Effects of Different Patterned Surface Geometries on Heat Transfer in A Rectangular Channel, *Tesisat Mühendisliği Dergisi*, 183, 37-49.
- Karabulut K., Alnak D. E., 2020, Study of Cooling of the Varied Designed Warmed Surfaces with An Air Jet Impingement, *Pamukkale Univ. J. Eng. Sci*, 26, 88-98.
- Karabulut K., Buyruk E., Kilinc F., 2020, Experimental and Numerical Investigation of Convection Heat Transfer in A Circular Copper Tube Using Graphene Oxide Nanofluid, *J. Braz. Soc. Mech. Sci. Eng.*, 42, 230.
- Karabulut K., 2019, Heat Transfer Improvement Study of Electronic Component Surfaces Using Air Jet Impingement, *J. Comp. Electronics*, 18, 1259-1271.
- Kılıç M., 2018, Investigation of Combined Effect of Nanofluids and Impinging Jets on Cooling of Electronic Systems, *Çukurova Univ J Fac Eng Arch*, 18, 121-132.
- Kilic M., Calisir T., Baskaya S., 2017, Experimental and Numerical Investigation of Vortex Promoter Effects on Heat Transfer from Heated Electronic Components in A Rectangular Channel with An Impinging Jet, *Heat Transf. Res.*, 48, 435-463.
- Kilic M., Calisir T., Baskaya S., 2016, Experimental and Numerical Study of Heat Transfer from A Heated Flat Plate in A Rectangular Channel with An Impinging Air Jet, *J. Braz. Soc. Mech. Sci. Eng.*, 39, 329-344.
- Kumar D., Zunaid M., Gautam S., 2021, Heat Sink Analysis in Jet Impingement with Air Foil Pillars and Nanoparticles, *Mater. Today: Proc.*, 46, 10752-10756.
- Ma C. F., Bergles A. E., 1983, Boiling Jet Impingement Cooling of Simulated Microelectronic Chips, *Heat Transf. Elect. Equ. HTD*, 28, 5-12.
- Maghrabie H. M., Attalla M., Fawaz H. E., Khalil M., 2017, Numerical Investigation of Heat Transfer and Pressure Drop of In-Line Array of Heated Obstacles Cooled by Jet Impingement in Cross-Flow, *Alexandria Eng. J.*, 56, 285-296.
- Masip Y., Rivas A., Larraona G. S., Anton R., Ramos J. C., Moshfegh B., 2012, Experimental Study of the Turbulent Flow Around A Single Wall-Mounted Cube Exposed to A Cross-Flow and An Impinging Jet, *Int. J. Heat Fluid Flow*, 38, 50-71.
- Maxwell J. C., 1873, *A Treatise on Electricity and Magnetism*, Clarendon Press, Oxford, United Kingdom.
- Mergen S., 2014, *Numerical Investigation of the Cooling of An Electronic Component with the Combination of Cross Flow and Impinging Jet*. MSc Thesis, University of Gazi, Ankara, Türkiye.
- Mohammed H. A., Gunnasegaran P., Shuaib N. H., 2011, The Impact of Various Nanofluid Types on Triangular Microchannels Heat Sink Cooling Performance, *Int. Commun. Heat Mass Transf.*, 3, 767-773.
- Naga Ramesh K., Karthikeya Sharma T., Amba Prasad Rao G., 2021, Latest Advancements in Heat Transfer Enhancement in the Micro-Channel Heat Sinks: A Review, *Arch. Comput. Methods Eng*, 28 (3), 135-3165.
- Nagesha K., Srinivasan K., Sundararajan T., 2020, Heat Transfer Characteristics of Single Circular Jet Impinging on A Flat Surface with A Protrusion, *Heat Mass Transf*, 56, 1901-1920.
- Öztürk S. M., Demircan T., 2022, Numerical Analysis of the Effects of Fin Angle on Flow and Heat Transfer Characteristics for Cooling An Electronic Component with Impinging Jet and Cross-Flow Combination, *J. Fac. Eng. Arch. Gazi Univ.*, 37, 57-74.
- Pak B. C., Cho Y. I., 1998, Hydrodynamic and Heat Transfer Study of Dispersed Fluids with Submicron Metallic Oxide Particles, *Exp. Heat Transf.*, 11, 151-170.
- Rathore S. S., Verma S. K., 2022, Numerical Investigation on the Efficacy of Jet Obliquity for Fluid Flow and Thermal Characteristics of Turbulent Offset Jet, *Heat Mass Transf*, 58, 1223-1246.
- Saleha N., Fadela N., Abbes A., 2015, Improving Cooling Effectiveness by Use Chamfers on the Top of Electronic Components, *Microelect. Reliab.*, 55, 1067-1076.
- Selimefendigil F., Chamkha A. J., 2020, Cooling of An Isothermal Surface Having A Cavity Component by Using CuO-Water Nano-Jet, *Int. J. Num. Methods Heat & Fluid Flow*, 30, 2169-2191.

Shi W., Li F., Lin Q., Fang G., 2021, Experimental Study on Instability of Round Nanofluid Jets at Low Velocity, *Exp. Therm. Fluid. Sci.*, 120, 110253.

Taylor J. R., 1997, *An Introduction to Error Analysis: The Study of Uncertainties in Physical Measurements*, University Science Books, Sausalito, United States of America.

Teamah M. A., Dawood M. M., Shehata A., 2015, Numerical and Experimental Investigation of Flow Structure and Behavior of Nanofluids Flow Impingement on Horizontal Flat Plate, *Exp. Therm. Fluid Sci.*, 74, 235-246.

Wang S. J., Mujumdar A. S., 2005, A Comparative Study of Five Low Reynolds Number $k-\epsilon$ Models for Impingement Heat Transfer, *App. Therm. Eng.*, 25, 31-44.

Zou L., Ning L., Wang X., Li Z., He L., Li H., 2022, Evaluation of Interfacial Heat Transfer Coefficient Based on the Experiment and Numerical Simulation in the Air-Cooling Process, *Heat Mass Transf.*, 58, 337-354.